ACS APPLIED

Enhancement of Nonlinear Optical Properties in Nb₂O₅-Modified Fluorophosphate Glasses

Artur Barbedo, José L. Clabel Huamán, L. Olivetti Estevam da Silva, Valmor R. Mastelaro, Lino Misoguti, Danilo Manzani, and Cleber R. Mendonça*



Cite This: https://doi.org/10.1021/acsaom.5c00298

OPTICAL MATERIALS



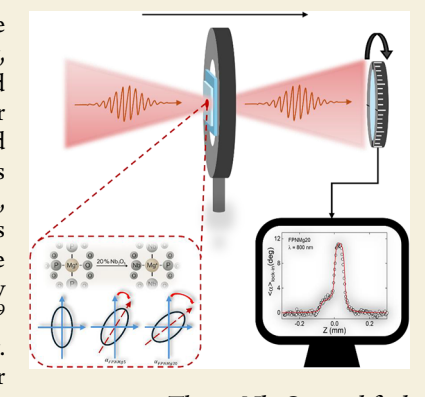
ACCESS I

Metrics & More

Article Recommendations

Supporting Information

ABSTRACT: Fluorophosphate glasses combine the beneficial features of both phosphate and fluoride networks. They exhibit high thermal and chemical stability, low hygroscopicity, low phonon energy, and a broad transparency window from ultraviolet UVI to near-infrared (NIR), making them attractive for advanced photonic applications. However, their nonlinear optical behavior has remained poorly explored, limiting their applicability for integrated photonics. The incorporation of heavy metal oxides (HMOs), such as Nb₂O₅, enables tailored structural and optical properties, enhancing third-order nonlinearities. In this work, the nonlinear refractive index (n2) of Nb2O5-modified fluorophosphate glasses was investigated using nonlinear elliptic rotation (NER) measurements, and the results were interpreted with the structural analyses obtained from X-ray photoelectron spectroscopy (XPS). A significant increase in n_2 was observed with Nb₂O₅ content, reaching 1.7×10^{-19} m²/W compared to 0.56×10^{-19} m²/W for samples with 20 and 5% content, respectively. XPS confirmed the progressive formation of nonbridging oxygen species (NBOs) over



bridging oxygens (BOs), directly correlating with enhanced polarizability and nonlinear response. Thus, Nb₂O₅-modified fluorophosphate glasses emerge as promising materials for nonlinear photonic applications, particularly in all-optical switching platforms, due to their good third-order optical figure of merit for photonic applications and favorable structural properties.

KEYWORDS: niobium oxide, fluorophosphate glasses, NERs technique, nonlinear refractive index, polarizability, XPS, nonbridging, bridging oxygens

1. INTRODUCTION

Glass is an essential material for cutting-edge applications and future technologies. 1,2 Their structural and compositional versatility allows them to be used in a wide range of applications, such as telecommunications, medicine, and integrated waveguides.⁵ One of the major areas of research in which glasses are widely used is photonics, presenting potential applications specifically related to their optical nonlinearities.⁵⁻⁷ Glasses have linear and nonlinear optical characteristics that are very interesting and, although they have already been studied extensively, still present innovations and challenges.8,9

Phosphate glasses are widely used due to their properties, such as thermal stability and transparency window in the ultraviolet-visible (UV-vis) and NIR. 10 Despite this, they presented some impasses that prevent them from being used as a single matrix, such as low chemical stability. 11 This has led to using alkaline earth metals to stabilize their matrix, which also incorporates other interesting properties into the glass. 12 These compounds can stabilize the phosphate network by breaking the P-O-P linkages and stabilizing the nonbridging oxygens (NBO). 13 For structural studies and nonlinear optics, the impact of NBOs on responses and their importance for different applications is well known, as they can be tunable in

different ways. 14 Additionally, as the phosphate matrix, the fluoride glass presents interesting properties such as low phonon energy; however, it has certain limitations regarding its low chemical and thermal stability. 15,16 To overcome these adversities, fluorophosphate matrices were developed, overcoming their problems and improving their qualities, also showing promising results for nonlinear optics. 12,17

It is also possible to improve some of the properties of these materials using network modifiers. The use of heavy metal oxides (HMOs), such as Bi₂O₃, WO₃, and Nb₂O₅, has been extensively studied. These compounds act as modifiers and can act as matrix formers, influencing the optical and chemical properties as much as the structural parameters. 18,19 In addition to increasing the optical density of the material and decreasing the bandgap, they also influence the structures to improve the nonlinear responses. As investigated by Komatsu et al., the influence of Nb2O5 in different glasses has relevant

Received: July 19, 2025 Revised: October 4, 2025 Accepted: October 5, 2025



structural roles, including in the enhancement of electronic polarizability and the linear refractive index of the samples. Also studied by Manzani et al., the addition of $\mathrm{Nb_2O_5}$ in different concentrations to phosphate matrices produced different responses, showing that not only does the addition play a fundamental role, but also controlling the concentration of modifiers in the matrix can have a significant influence. ¹¹

Therefore, we systematically studied linear and nonlinear optical properties in four new fluorophosphate glasses with different percentages of $\mathrm{Nb_2O_5}$ in the composition. We used the nonlinear elliptic rotation (NER) method to determine the nonlinear refractive index ($\mathrm{n_2}$). This technique enables excitation wavelength variation, which is essential to figure out the photonics application potential over a broad wavelength range. In addition, structural characterizations, such as Raman spectroscopy and XPS, were performed to better understand the influence of the modifiers in this matrix and the origins of the material's different optical responses. Finally, an analysis of the material's figures of merit was carried out with a focus on all-optical switching applications, with promising results.

2. EXPERIMENTAL SECTION

Six grams batch of each glass sample was synthesized by the conventional melt-quenching method, according to the composition, in mol %, $(80-y)(\mathrm{NaPO_3})_n-(y)\mathrm{Nb_2O_5}$ -20MgF₂, y=5, 10, 15, and 20. Samples were labeled as FNPMg5, FNPMg10, FNPMg15, and FNPMg20 according to the percentage of Nb₂O₅ in the composition. The optical grade reagents, $(\mathrm{NaPO_3})_n$ 65–70% P₂O₅ basis (Aldrich), MgF₂ (Aldrich), and Nb₂O₅ (CBMM) were first weighed and homogenized in an agate mortar, transferred to a Pt/Au (95/5 mol %) crucible covered with a lid, and submitted to melting in an electric furnace (EDG 3000) at 1075 °C for 30 min. After the melting, the liquid was poured into a preheated stainless-steel mold at 300–350 °C (depending on the composition) for 4 h to release mechanical stress, followed by slow cooling to room temperature. The obtained samples were cut into pieces and polished until around 1 mm thick for optical characterization.

We used the Archimedes method to determine the density of the samples at room temperature. Immersion was performed in anhydrous ethanol. We acquired the linear optical absorption spectra between 200 and 1100 nm, for all samples, with a Shimadzu 18,000 spectrometer and calculated the bandgap using the Tauc plot method.²¹ Additionally, structural measurements were performed to enhance our understanding of how niobium oxide, as a modifier, affects the glass matrix. Surface chemical analysis of the glass samples was carried out by X-ray photoelectron spectroscopy (XPS) at ambient temperature using an ESCA+ Omicron-Scienta spectrometer equipped with a monochromatic Al K α source ($h\nu$ = 1486.6 eV) under a base pressure of ~10⁻⁹ Torr. No sputtering was applied. High-resolution spectra were acquired with a pass energy of 30 eV and a step size of 0.05 eV, while survey scans used 50 and 0.5 eV, respectively. The emission angle was 54.7°, and the analyzed area was \sim 200 μ m². Charge neutralization was achieved using an electron flood gun (<1.6 eV). Spectra were processed using CasaXPS software (Casa Software Ltd., U.K.) with Shirley background subtraction, and the C 1s peak at 284.6 eV was used for binding energy calibration.

We have used the self-reference NER technique to measure the nonlinear refractive index (n_2) of the samples. ²² In this technique, we used fused silica as a reference sample, which has a well-known n_2 (2.5 \times 10⁻²⁰ m²/W), considered constant over the studied wavelength range. ²³ This measurement required a femtosecond laser system (Pharos–Light Conversion, 1030 nm, 190 fs, 7.5 kHz) pumping an optical parametric amplifier (Orpheus–Light Conversion), allowing wavelength variation between 700 and 1500 nm. After passing through a rotating polarizer, the output signal is collected by using a silica or germanium detector connected to a dual-phase lock-in,

depending on the wavelength. The experimental data were collected and analyzed using a National Instruments acquisition system and LabVIEW software, respectively. Further details on the experimental setup and methodology can be found in ref 22,24.

3. RESULTS AND DISCUSSION

3.1. Physical Properties

The density of the glasses, presented in Figure 1, shows a direct relationship with the addition of Nb_2O_5 in the

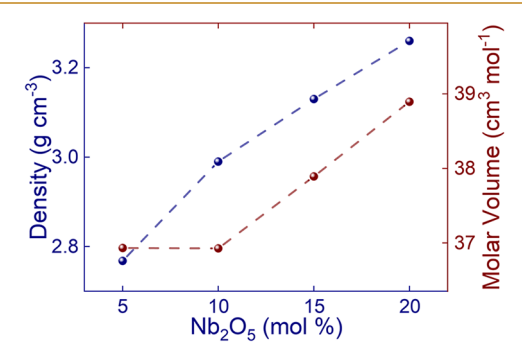


Figure 1. Density of the glasses as a function of the percentage of $\mathrm{Nb}_2\mathrm{O}_5$ in the composition (blue circle) presents a linear dependence. The molar volume (red circle) plotted with $\mathrm{Nb}_2\mathrm{O}_5$ presents a similar behavior to the density.

composition, reaching an increase of approximately 18%, from 2.8 g cm⁻³ (FPNMg5) to 3.3 g cm⁻³ (FPNMg20). This is related to the change in NaPO₃, which has a lower molar mass of approximately 102.0 g mol⁻¹, compared to that of the modifier Nb₂O₅, with a molar mass of around 265.8 g mol⁻¹. The molar volume (Figure 1) is determined by $V_{\rm m} = \frac{M}{\rho}$, indicating a similar density behavior, reaching 38.9 m³ mol⁻¹ for the glass with the highest percentage of Nb₂O₅, compared to 36.9 cm³ mol⁻¹ on the glass with the lowest modifier. This indicates that the modifier acts on the glass matrix not only by expanding the structure but also by increasing the density of the glass, which can influence the optical responses.

The thermal behavior of the FPNMg glasses was previously investigated via differential scanning calorimetry (DSC). The measured values, summarized in Table S1 and Supporting Figure S1, show that the glass transition temperature (T_g) increases with Nb₂O₅ content from 359 to 485 °C. This trend reflects enhanced network connectivity and thermal stability ($\Delta T = T_X - T_g$), which are advantageous for the fabrication of nonlinear photonic components.

The molar volume of oxygen $(V_{\rm O})$ and the oxygen packing density (OPD), displayed in Table 1, were determined using the following equations: 26 $V_{\rm O} = \frac{V_{\rm m}}{\sum_i c_i n_i}$, and OPD = $1000 \frac{C_{\rm O}}{V_{\rm m}}$,

where M is the molar mass, c_i is the mol % of each component, n_i is the number of oxygen atoms per formula unit, C_0 is the total number of oxygen atoms per formula unit. Although there is a rise in mol % of oxygen atoms in the matrix, the molar volume of oxygen decreases, indicating a higher density of oxygen, which agrees with the increase in the glass density. The increase in the level of the OPD confirms these results, proving that there is more oxygen per volume in the sample. Furthermore, we analyzed the molar electronic polarizability $(\alpha_{\rm M})$, which is defined by eq 1.

Table 1. Chemical Composition (in %), Density (in g·cm⁻³), Molar Volume (in cm³·mol⁻¹), Molar Volume of Oxygen V_O (cm³·mol⁻¹), Oxygen Packing Volume, Oxygen Packing Volume, OPD (g·atom·L⁻¹), and Molar Electronic Polarizability α_M (×10⁻²⁴ cm³)

sample	chemical composition (%)	density $(g.cm^{-3})$	molar volume (cm ³ .mol ⁻¹)	$V_{\rm O}~({ m cm}^3/{ m mol}~{ m O})$	OPD (mol O/cm ³)	$\alpha_{\rm M}~(\times 10^{-24}~{\rm cm}^3)$
FPNMg5	$75(NaPO_3)-5Nb_2O_5-20MgF_2$	2.8 ± 0.2	36.9 ± 0.3	14.77 ± 0.04	67.7 ± 0.2	1.57 ± 0.09
FPNMg10	$70(NaPO_3)-10Nb_2O_5-20MgF_2$	3.0 ± 0.2	36.9 ± 0.2	14.20 ± 0.03	70.4 ± 0.2	1.76 ± 0.09
FPNMg15	$65(NaPO_3)-15Nb_2O_5-20MgF_2$	3.1 ± 0.2	37.9 ± 0.2	14.03 ± 0.03	71.3 ± 0.2	2.0 ± 0.1
FPNMg20	$60 (NaPO_3) - 20 Nb_2 O_5 - 20 MgF_2$	3.3 ± 0.2	38.9 ± 0.2	13.89 ± 0.03	72.0 ± 0.2	2.3 ± 0.1

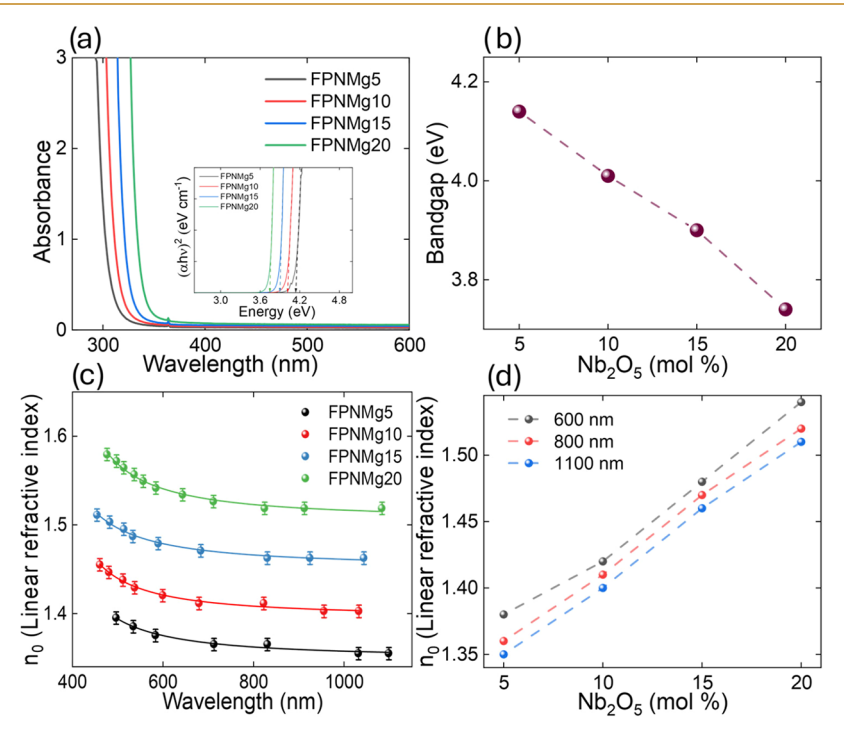


Figure 2. (a) Absorption spectra of the samples with increasing Nb₂O₅ content (from FPNMg5 to FPNMg20). The inset shows the Tauc plot used to estimate the direct bandgap. (b) Optical bandgap as a function of Nb₂O₅ concentration. (c) Sellmeier fits for the dispersion of linear refractive index between 650 and 1100 nm for all compositions. (d) Refractive index (n_0) values at 600 nm (black), 800 nm (red), and 1100 nm (blue) as a function of Nb₂O₅ content.

$$\alpha_{\rm M} = \left(\frac{3}{4\pi N_{\rm A}}\right) R_{\rm M} \tag{1}$$

in which $N_{\rm A}$ is Avogadro's number, $R_{\rm M}$ is the molar refraction value, given by the Lorentz-Lorenz equation $R_{\rm M} = \left| \frac{n_0^2 - 1}{n_0^2 + 2} \right| \frac{M}{\rho}$ n_0 is the linear refractive index, M is the molecular weight, and ρ is the density (displayed in Table 1). $\alpha_{\rm M}$ is an important parameter for evaluating and better understanding glasses' linear and nonlinear optical responses. The increase presented in $\alpha_{\rm M}$ can be related to the previously presented change in the glass density, given by the addition of heavy elements to the composition. These results can also be attributed to the high polarizability of Nb5+, and the NbO6 octahedra distortion in the glass. 19 The substitution of the components leads to an enhancement of the sample's polarizability, which improves the nonlinear responses.^{27,28} Additionally, this improvement may be linked to the nonbridging oxygens (NBO) formation in the samples. The addition of niobium oxides in the composition may influence the structure to transform bridging oxygens (BO) into NBO, which is reported to be more polarizable.¹⁴

3.2. Linear Optical Properties

The linear absorption spectrum of glasses is shown in Figure 2a, revealing a wide transparency window from 400 to 1100 nm. A red shift in the absorption edge occurs as the percentage of the modifier increases. This shift indicates that the optical bandgap decreases with the addition of Nb₂O₅. We estimated these values using the Tauc plot method for the bandgap calculation, assuming a direct transition. The E_{GAP} values are displayed in Figure 2b, where the FPNMg5 shows a bandgap of approximately 4.14 eV, which decreases with the addition of the oxide, reaching 3.75 eV for FPNMg20, consistent with the UV—vis spectra. As observed in the studies of Manzani et al., 11 Faleiro et al., 18 and Chu et al., 29 the decrease can be associated with the formation of NBO in the structure. The formation of NbO₆ octahedra, caused by the addition of Nb₂O₅, improves the connectivity and polarizability of the glass network and contributes to a higher concentration of NBO. 30 Moreover, the Nb⁵⁺ cations, with a larger ionic radius than P⁵⁺, interfere more with the NBO, inducing defects and decreasing the bandgap.

By measuring the Fresnel reflections in the range without absorption, we determined the linear refractive index n_0 of the samples, which was fit using the Sellmeier equation in a bipolar approximation. Figure 2c displays the dispersion of n_0 as a function of wavelength, with values ranging from 1.36 for

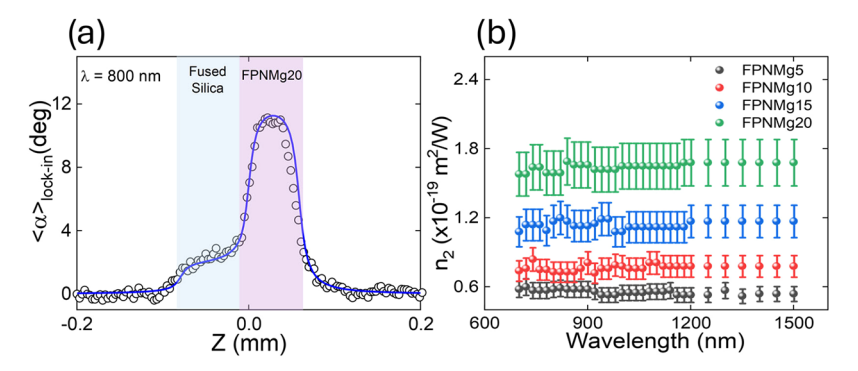


Figure 3. (a) NERS measurement and theoretical fit of the nonlinear refractive index at 800 nm for FPNMg20, showing two plateaus corresponding to fused silica and the sample. (b) Nonlinear refractive index as a function of wavelength from FPNMg5 to FPNMg20, revealing a linear trend within experimental uncertainty.

FPNMg5 to 1.52 for FPNMg20. Such values are relatively low compared to other phosphate glasses. The n_0 can be linked to the electron density of the matrix, in this case, related to the niobium atoms with an extended electron cloud, due to its valence configuration. Furthermore, the presence of oxygen in the glass can play an important role in refractive index. In this composition, the breaking of P-O-P linkages in the phosphate glasses happens with the addition of Nb₂O₅, increasing the presence of NBO. As mentioned before, these NBOs are more polarizable, inducing higher n_0 . This behavior was previously discussed by Sene et al. in a similar niobium phosphate glass. Besides that, this augmentation in the refractive index, shown in Figure 2d, may be attributed to higher density values with the augmentation of HMO and the rise in the polarizability upon exchange of niobium oxide.

3.3. Nonlinear Optical Properties

The self-referenced NER technique allows us to measure the $\rm n_2$ of our samples with high precision. This technique correlates the induced phase shift of elliptically polarized intense light with the nonlinear refractive index, when focused on a nonlinear medium. This relationship is given by eq 2.

$$\langle \alpha(z) \rangle_{\text{lock-in}} = \frac{1}{\sqrt{2}} \frac{\omega}{c} \frac{\sin(2\varphi)}{2} \left(\frac{2n_2}{3}\right) (n_0 z_0) I_0$$

$$\left[tg^{-1} \left(\frac{z_B}{z_0}\right) - tg^{-1} \left(\frac{z_A}{z_0}\right) \right]$$

$$(2)$$

where $z_{\rm B}=z+L/(2n_0)$ and $z_{\rm A}=z-L/(2n_0)$, L is the sample length, ω is the laser frequency, c is the speed of light, n_0 is the linear refractive index, I_0 is the laser irradiance, and φ is the angle of the quarter-wave plate. With the quarter-wave plate, we can vary the polarization of the light between linear polarization (0°) and circular polarization (45°) and, in this case, an elliptical laser beam ($\sim 22^{\circ}$). We used fused silica as a reference sample that is attached to the interested sample, enabling the measurement of both in a single scan and guaranteeing the same experimental parameters. The induced phase shift is illustrated in Figure 3a, where the circles represent our experimental results, and the red line indicates the theoretical fit, one corresponding to the sample of interest and the other to the fused silica at 800 nm. In Figure 3b, we summarize the dispersion of n₂ from all samples from 700 to 1500 nm, presenting a linear behavior in all cases, and no nonlinear absorption. With the addition of more Nb₂O₅ in the composition, the mean values of the glasses increase from 0.56 $\times 10^{-19} \text{ m}^2/\text{W}$ in FPNMg5 to 1.7 $\times 10^{-19} \text{ m}^2/\text{W}$ in FPNMg20, exhibiting a significant positive influence on nonlinear response due to the modifier, as observed in the linear measurements. The enhanced NBO concentration, caused by the addition of $\mathrm{Nb_2O_5}$ in the matrix, induces a higher-density environment, as well as increased polarizability of the material, ^{31,35} leading to higher nonlinear responses. The obtained values present $\mathrm{n_2}$ in the same order as compositions in the same field, such as tellurites ³⁶ and borate, ^{37,38} and higher than other conventional glasses. ³⁹

The correlation between n_2 and the electronic molar polarizability is evidenced by the linear behavior displayed in Figure 4.

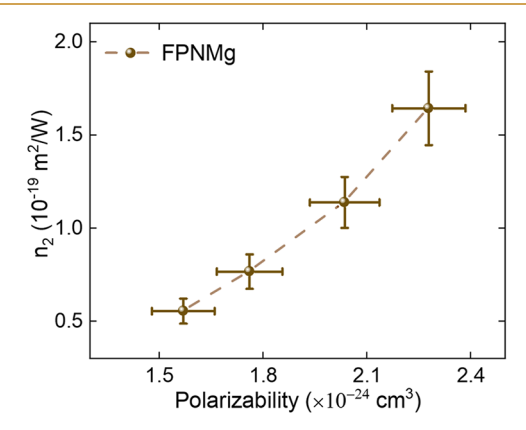


Figure 4. Mean value of nonlinear refractive index between 700 and 1500 nm as a function of the electronic molar polarizability, presenting a linear dependence of them.

This high polarizability can induce higher nonlinear responses, as presented in this work and in studies with different compositions, such as presented by Clabel et al. and Azlan et al. for the tellurite glasses, ^{40,41} and by Manzani *et al.* for phosphate glasses doped with niobium oxide. ¹¹ The last one, with a similar composition and modifier, assigned the increase in the polarizability to the formation of NbO₆ octahedra, augmenting the network polarizability due to the increase of terminal oxygen atoms, besides the extended electron cloud of the *d* orbital of the formed Nb⁴⁺. Therefore, our results indicate that the combination of these structural modifications and the formation of NBO results in higher nonlinear responses. This evidence shows the importance of HMO as a modifier to enhance the linear and nonlinear properties of glasses.

ACS Applied Optical Materials

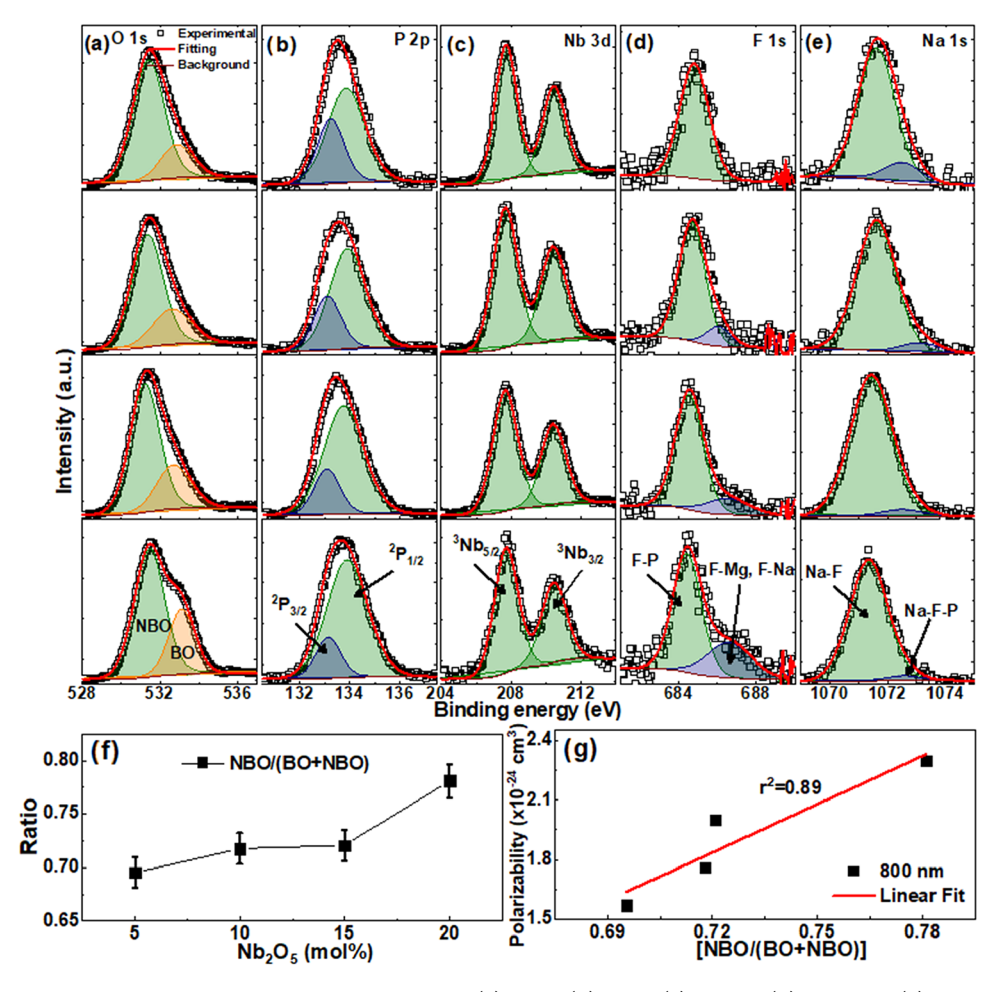


Figure 5. XPS spectra of high resolution and deconvoluted spectra of (a) O 1s, (b) P 2p, (c) Nb 3d, (d) F 1s, and (e) Na 1s for FPNMg glasses with increasing Nb_2O_5 content (from bottom to top: 5, 10, 15, and 20 mol %). (f) Relationship between Nb_2O_5 (mol %) and ratio (NBO/BO + BNO). (g) Relation between polarizability and Nb_2O_5 (mol %) content as a function of nonbridging oxygen.

3.4. XPS Analysis

X-ray photoelectron spectroscopy (XPS) was employed to investigate the surface chemical environments and elemental stoichiometry of FPNMg glasses, aiming to elucidate the structural rearrangements that modulate their third-order nonlinear optical (NLO) response. High-resolution spectra of O 1s, P 2p, Nb 3d, F 1s, and Na 1s were acquired for glasses with varying Nb₂O₅ content, with binding energies calibrated using the C 1s peak of graphitic carbon at 284.8 eV. 42 Systematic shifts and intensity variations reveal progressive changes in the bonding environments. Complementarily, atomic percentages of F, O, P, Na, Mg, and Nb were extracted from XPS survey spectra and are summarized in Table S2 (Supporting Information). These data confirm progressive Nb incorporation and effective retention of fluoride, validating the reliability of surface-sensitive XPS for tracking compositional trends across the glass series.

The spectra of the O 1s (Figure 5a) were deconvoluted into two components. The peak at 531.3 eV was assigned to nonbridging oxygen (NBO) species associated with environments such as P-O-F and P-O-M (M=Na⁺, Mg²⁺), along with possible contributions from surface M-OH and C-O bonds. The peak at 532.7 eV was attributed to bridging oxygen (BO) species in P-O-P bonds. Initially, NBO species predominated due to the network depolymerization induced by MgF₂ (20 mol %). With increasing Nb₂O₅ content

(5 to 20 mol %), a progressive reorganization occurred: BO content decreased slightly, while NBO content increased, suggesting the formation of P-O-Nb bonds; see Figure 5f.

To quantitatively probe the local bonding environment, average M–O bond lengths $(R_{\rm M-O})$ were estimated from the O 1s binding energies using the empirical relation $R_{\rm M-O}({\rm nm}) = 2.27(E_{\rm b}-519.4)^{-1}.^{44}$ The BO component exhibited a slight contraction from ~0.182 nm to 0.178 nm with increasing Nb₂O₅, whereas the NBO component remained nearly constant at ~0.16–0.17 nm. This trend suggests that the formation of P–O–Nb bonds results in shorter and stronger bridging environments, corroborating the structural reorganization inferred from the spectral evolution.

This structural reorganization is corroborated by the P 2p spectra (Figure 5b), which exhibit spin—orbit splitting into two peaks at 133.1 eV ($^2\mathrm{P}_{3/2}$) and 133.9 eV ($^2\mathrm{P}_{1/2}$), corresponding to chemically distinct phosphorus environments. The $^2\mathrm{P}_{1/2}$ component corresponds to bridging configurations (P–O–P bonds, P–O–Nb bonds), while the $^2\mathrm{P}_{3/2}$ peak is attributed to terminal bonds such as P=O and P–F. Sodium and magnesium act as charge compensators without forming covalent bonds with oxygen. The increase in the ($^2\mathrm{P}_{3/2}$)/ ($^2\mathrm{P}_{1/2}$) intensity ratio, from 0.12 (5 mol % Nb₂O₅) to 0.50 (20 mol %), confirms the progressive formation of P–O–Nb linkages with increasing Nb content.

These trends align with Raman spectroscopy results (see ref 25), which revealed growing contributions of depolymerized phosphate units. In particular, bands near ca. 970–990 and $1080-1120~{\rm cm}^{-1}$, assigned to Q¹ and Q⁰ units, respectively, intensified with Nb₂O₅ content, while no distinct Q² signature was detected. This behavior corroborates the increasing NBO/BO ratio and supports a structural model based on network depolymerization and Nb-driven cross-linking.

The Nb 3d spectra (Figure 5c) exhibit two well-defined peaks at ~207.2 and ~210.0 eV, assigned to Nb 3 d_{5/2} and Nb 3 d_{3/2}, respectively, characteristic of Nb⁵⁺. The absence of Nb⁴⁺ or Nb³⁺ peaks indicates that Nb is stably incorporated into the network, reinforcing the bonding environment changes inferred from the diffraction analyses of the O 1s and P 2p analyses. The F 1s spectra (Figure 5d) show two components at 686.6 and 684.4 eV, corresponding to covalent P–F bonds and ionic associations with modifier cations (F–Mg, F–Na), respectively. With increasing Nb₂O₅ content, the P–F component intensifies, while the F–Mg and F–Na contributions diminish, reflecting enhanced fluoride integration into the glass network.

This interpretation is supported by complementary spectroscopic data: Raman spectra (Supporting Information, Figure S2) display a vibrational band near ~896 cm⁻¹, attributed to P–F stretching modes, while ¹⁹F MAS NMR reveals a dominant resonance between –120 and –140 ppm, consistent with fluorine covalently bonded to phosphorus. No signals indicative of Nb–F or free F⁻ species were observed, validating the XPS-based assignment of fluoride environments.

Furthermore, the Na 1s spectra (Figure 5e) reveal two contributions between 1070 and 1074 eV: Na–F interactions (~1071 eV) and Na⁺ ions were associated with fluorinated phosphate groups (Na–F–P, ~1073 eV). As the Nb₂O₅ content increases, the Na–F contribution decreases, while the Na–F–P signal becomes more prominent, reflecting the network reorganization involving P–O–Nb bond formation and enhanced fluoride incorporation into the phosphate framework.

The structural evolution of FPNMg glasses involves two key processes. First, fluoride ions depolymerize the phosphate network by breaking P-O-P bridges and forming terminal P-F bonds, according to eq 3

$$P - O - P + 2F^{-} \rightarrow 2P - F + O^{2-}$$
 (3)

Subsequently, ${\rm Nb_2O_5}$ incorporation promotes network repolymerization via cross-linking P-O-Nb-O-P bonds, according to eq 4

$$P - O - P + Nb_2O_5 \rightarrow 2P - O - Nb - O - P$$
 (4)

These complementary processes account for the observed increase in P–F and P–O–Nb bonding, the shift in NBO/ (NBO + BO) ratios, and the reorganization of modifier cation environments. To assess their influence on the nonlinear response, the relationship between network structure and electronic polarizability was analyzed (Figure 5g), revealing a strong linear correlation ($r^2 = 0.89$) between polarizability and the NBO fraction. Since the nonlinear refractive index n_2 is directly proportional to electronic polarizability, the increase in NBO sites, stabilized by Nb⁵⁺ and F⁻, effectively enhances third-order nonlinearities. This structural-optical synergy aligns with previous findings in tellurite and phosphate glasses doped with high-polarizability cations (e.g., Nb, Bi). ^{14,26} Altogether, these results establish Nb₂O₅ as an effective network modifier

for tuning both the structure and nonlinear optical performance in fluorophosphate systems.

3.5. Applications for All-Optical Switching

Considering the high nonlinear responses of the material, which can be tuned by varying the concentration of niobium oxides, its high chemical stability, and its high density, the samples are excellent candidates for various applications. One important application involving glasses is optical communications, where high n₂ with precise control is required. To this end, three parameters for evaluating their potential are displayed here. The first one is $W = \frac{\bar{\Delta n}}{\lambda \alpha_0}$ with $\Delta n = n_2 I$, I the laser irradiance, λ the wavelength, and α_0 the linear absorption coefficient. The second figure of merit is the T, described by $T = \frac{\beta \lambda}{n}$, where β is the two-photon absorption coefficient. The NER technique enables acquiring the transmittance change, ΔT , from which we can calculate $\beta \approx 2^{3/2} \Delta T/IL$, with L the effective thickness of the sample given by $L = n_0 z_0$, where n_0 is the linear refraction index and z_0 is the Rayleigh length. Hence, the third figure of merit can be determined by eq 5.

$$FOM_{2PA} = \frac{4\pi}{\lambda} \left| \frac{n_2(\omega)}{\beta(\omega)} \right| \tag{5}$$

For different applications, such figures of merit should be higher than certain specific thresholds. For example, for Mach–Zehnder interferometers, FOM > 4π and W > 0.5 are needed. However, the criterion for other all-optical switching applications is W > 1 and T < 1. Table 2 summarizes the values we obtained for the samples studied here.

Table 2. Mean Value of the Nonlinear Refractive Index is from 700 to 1500 nm (10^{-19} m²/W), Two-Photon Absorption Coefficients (10^{-14} m/W), Figure W, and Figure of Merit (FOM_{2PA})

samples	$n_2 \left(\times 10^{-19} \right) \atop \text{m}^2/\text{W}$	$\beta \ (\times 10^{-13}) \ \text{m/W}$	W (1100 nm)	FOM _{2PA} (700 nm) (π)
FPNMg5	0.56 ± 0.06	1.3 ± 0.3	3.1 ± 0.4	(3 ± 2)
FPNMg10	0.77 ± 0.09	1.9 ± 0.4	2.2 ± 0.3	(2 ± 1)
FPNMg15	1.1 ± 0.1	1.0 ± 0.2	2.5 ± 0.3	(6 ± 2)
FPNMg20	1.7 ± 0.2	1.6 ± 0.3	1.8 ± 0.2	(6 ± 2)

Because *W* compares the nonlinear refractive index with the linear absorption of the material, care is needed in terms of which wavelength is used. Close to the absorption edge are localized Urbach states, which explain the tail at the edge of the absorption spectrum. Thus, the values of the linear absorption coefficient can mislead the analysis. With that in mind, this figure of merit was studied at 1100 nm, enabling different application possibilities. In all cases, the best response was obtained for FPNMg5, due to its very low absorption coefficient compared to other glasses, although all of them have considerable values for possible applications.

By leveraging the Urbach states, we studied the second and third figures of merit that relate the nonlinear refractive index to the two-photon absorption coefficient. The two-photon absorption associated with these states occurs within the Urbach tails, which extend to approximately 350 nm, enabling the examination of β up to 700 nm. The values found for T vary from 1.6 to 0.7 with the addition of more modifiers, with FPNMg15 and FPNMg20 presenting values smaller than 1,

being 1.6 for FPNMg5, 1.7 for FPNMg10, 0.64 for FPNMg15, and 0.67 for FPNMg20. Besides that, the FOM $_{\rm 2PA}$ reveals that glasses with Nb $_{\rm 2}O_{\rm 5}$ concentrations above 15% display values higher than those required for different applications. Both FPNMg15 and FPNMg20 present similar values for FOM $_{\rm 2PA}$, attributed to the fact that although the second presents a higher $\rm n_2$ value, its two-photon absorption coefficient also increases. Our experiments demonstrated no evidence of nonlinear absorption at longer wavelengths. Consequently, the FOM values can be elevated due to the high noise/signal ratio in these cases, stemming from the minimal variation in transmission during the experiment.

4. CONCLUSION

In this work, we presented the enhancement of fluorophosphate glasses' physical and optical properties by incorporating heavy metal oxides, specifically niobium oxide, in varying percentages. The addition and concentration of the modifiers can lead to interesting properties, such as a high linear and nonlinear refractive index and robust chemical and thermal stability. Varying from 5% of Nb₂O₅ to 20% in the composition, there was an increase in the nonlinear refractive index from $0.56 \times 10^{-19} \text{ m}^2/\text{W}$ in FPNMg5 to $1.7 \times 10^{-19} \text{ m}^2/\text{W}$ W in FPNMg20. Through XPS results, we confirmed that these changes are related to the formation of NBO in the samples, which is extensively presented as an enhancer of nonlinear properties. With the high values of n2, aligned with their optimal structural properties, we discussed different figures of merit, aiming at the applicability of the samples in photonics. The results shown for FPNMg15 and FPNMg20 confirm their possible applications in all-optical switching and other photonic devices.

ASSOCIATED CONTENT

Supporting Information

The Supporting Information is available free of charge at https://pubs.acs.org/doi/10.1021/acsaom.5c00298.

Complementary data to the main manuscript, including thermogram obtained by DSC of the samples with increasing Nb₂O₅ content (from FPNMg5 to FPNMg20), Raman spectra of FPNMg glasses showing the P–F stretching band (~896 cm⁻¹) and the evolution of phosphate Q⁰ (1080–1120 cm⁻¹) and Q¹ (~970–990 cm⁻¹) units with increasing Nb₂O₅ content, and ¹⁹F MAS NMR spectra with a dominant P–F resonance (–120 to –140 ppm) adapted from ACS Omega, DOI: 10.1021/acsomega.5c05892. 2025 The Authors; published by the American Chemical Society; published under the terms of the Creative Commons CC BY 4.0 license; atomic percentages (at.%) of constituent elements from XPS survey spectra for FPNMg glasses (PDF)

AUTHOR INFORMATION

Corresponding Author

Cleber R. Mendonça — São Carlos Institute of Physics, University of São Paulo, (USP), São Carlos, SP 13560-970, Brazil; ⊚ orcid.org/0000-0001-6672-2186; Email: crmendon@ifsc.usp.br

Authors

Artur Barbedo — São Carlos Institute of Physics, University of São Paulo, (USP), São Carlos, SP 13560-970, Brazil José L. Clabel Huamán — São Carlos Institute of Physics, University of São Paulo, (USP), São Carlos, SP 13560-970, Brazil; ⊚ orcid.org/0000-0002-7413-4795

L. Olivetti Estevam da Silva — São Carlos Institute of Chemistry, University of São Paulo (USP), São Carlos, SP 13560-970, Brazil; © orcid.org/0000-0001-9241-1285

Valmor R. Mastelaro — São Carlos Institute of Physics, University of São Paulo, (USP), São Carlos, SP 13560-970, Brazil; orcid.org/0000-0001-9512-4214

Lino Misoguti — São Carlos Institute of Physics, University of São Paulo, (USP), São Carlos, SP 13560-970, Brazil;
orcid.org/0000-0001-6624-8453

Danilo Manzani — São Carlos Institute of Chemistry, University of São Paulo (USP), São Carlos, SP 13560-970, Brazil; © orcid.org/0000-0001-7280-5404

Complete contact information is available at: https://pubs.acs.org/10.1021/acsaom.5c00298

Funding

The Article Processing Charge for the publication of this research was funded by the Coordenacao de Aperfeicoamento de Pessoal de Nivel Superior (CAPES), Brazil (ROR identifier: 00x0ma614).

Notes

The authors declare no competing financial interest.

ACKNOWLEDGMENTS

This research was supported by the São Paulo Research Foundation (FAPESP), grants 2018/11283-7, 2021/11484-5, 2022/01762-0, 2023/09794-1, 2024/17334-3, and 2024/00905-8; Conselho Nacional de Desenvolvimento Científico e Tecnológico (CNPq), grants 405048/2021-1, 440225/2021-3, 312802/2023-4, and 304718/2023-08; Army Research Laboratory (W911NF-17-1-0123, W911NF-21-1-0362); and Air Force Office of Scientific Research (FA9550-23-1-0664).

REFERENCES

- (1) Bennett, T. D.; Horike, S.; Mauro, J. C.; Smedskjaer, M. M.; Wondraczek, L. Looking into the Future of Hybrid Glasses. *Nat. Chem.* **2024**, *16* (11), 1755–1766.
- (2) Blanc, W.; Gyu Choi, Y.; Zhang, X.; Nalin, M.; Richardson, K. A.; Righini, G. C.; Ferrari, M.; Jha, A.; Massera, J.; Jiang, S.; Ballato, J.; Petit, L. The Past, Present and Future of Photonic Glasses: A Review in Homage to the United Nations International Year of Glass 2022. *Prog. Mater. Sci.* 2023, 134, No. 101084.
- (3) Mehaboob, A.; Fuertes, V.; Rivera, V. A. G.; Messaddeq, Y. Tailoring Ultrabroadband Near-infrared Luminescence in Bi-Doped Germanosilicate Glasses. *Sci. Rep* **2023**, *13* (1), No. 22852.
- (4) Chen, X.; Chen, X.; Pedone, A.; Apperley, D.; Hill, R. G.; Karpukhina, N. New Insight into Mixing Fluoride and Chloride in Bioactive Silicate Glasses. *Sci. Rep.* **2018**, 8 (1), No. 1316.
- (5) Choi, J. W.; Han, Z.; Sohn, B.-U.; Chen, G. F. R.; Smith, C.; Kimerling, L. C.; Richardson, K. A.; Agarwal, A. M.; Tan, D. T. H. Nonlinear Characterization of GeSbS Chalcogenide Glass Waveguides. *Sci. Rep.* **2016**, *6* (1), No. 39234.
- (6) Huang, C.; Luo, Y.; Zhao, Y.; Ma, X.; Yan, Z.; Liu, Z.; Sheng, C.; Zhu, S.; Liu, H. A Conformal Mapping Approach to Broadband Nonlinear Optics on Chip. *Nat. Photonics* **2024**, *18* (5), 471–477.

- (7) Taha, E. O.; Saeed, A. The Effect of Cobalt/Copper Ions on the Structural, Thermal, Optical, and Emission Properties of Erbium Zinc Lead Borate Glasses. *Sci. Rep.* **2023**, *13* (1), No. 12260.
- (8) Clabel H, J. L.; Lozano C, G.; Pinto, I. C.; Falci, R. F.; Rivera, V. A. G.; Messaddeq, Y.; Marega, E. Overall Aspects of Glasses for Photonic Devices. *Adv. Glass Res.* **2023**, 1–52.
- (9) Tao, H.; Bennett, T. D.; Yue, Y. Melt-Quenched Hybrid Glasses from Metal-Organic Frameworks. *Adv. Mater.* **2017**, 29 (20), No. 1601705.
- (10) Muñoz, F.; Rocherullé, J.; Ahmed, I.; Hu, L. Phosphate Glasses. In *Springer Handbooks*; Springer, 2019; pp 553–594.
- (11) Manzani, D.; Gualberto, T.; Almeida, J. M. P.; Montesso, M.; Mendonça, C. R.; Rivera, V. A. G.; De Boni, L.; Nalin, M.; Ribeiro, S. J. L. Highly Nonlinear Pb₂P₂O₇-Nb₂O₅ Glasses for Optical Fiber Production. *J. Non Cryst. Solids* **2016**, *443*, 82–90.
- (12) Möncke, D.; Eckert, H. Review on the Structural Analysis of Fluoride-Phosphate and Fluoro-Phosphate Glasses. *J. Non Cryst. Solids: X* **2019**, *3*, No. 100026.
- (13) da Silva, L. O. E.; Rivera, V. A. G.; Falci, R.; Messaddeq, Y.; de Oliveira Junior, M.; Manzani, D. Fluorine Alkaline Earth (MgF₂, CaF₂, SrF₂, BaF₂) Influence on Thermal, Structural, and Luminescent Properties of Eu³⁺-Doped Niobium Phospho-Fluoride Glass. *Mater. Res. Bull.* **2025**, *185*, No. 113291.
- (14) Clabel H, J. L.; Lozano, G.; Marega, E.; Rivera, V. A. G. XPS Analysis of Bridging and Non-Bridging Oxygen in Yb³⁺-Er³⁺-Tm³⁺-Doped Zinc-Tellurite Glasses. *J. Non Cryst. Solids* **2021**, 553, No. 120520.
- (15) Poulain, M.; Cozic, S.; Adam, J. L.Fluoride Glass and Optical Fiber Fabrication. In *Mid-Infrared Fiber Photonics: Glass Mater, Fiber Fabrication & Process, Laser & Nonlinear Sources*; Woodhead Publishing, 2022; pp 47–109.
- (16) Zhu, H.; Chen, H.; Sun, Q.; Zhang, J.; Sheng, J. Study on the Mechanism of Potassium Fluoride, Magnesium Fluoride and Calcium Fluoride on the Crystal Morphology and Sintering Performance of Fluorapatite Functional Glass-Ceramics. *Ceram. Int.* **2024**, *50* (22), 45300–45310.
- (17) De Oliveira, M.; Gonçalves, T. S.; Ferrari, C.; Magon, C. J.; Pizani, P. S.; De Camargo, A. S. S.; Eckert, H. Structure-Property Relations in Fluorophosphate Glasses: An Integrated Spectroscopic Strategy. *J. Phys. Chem. C* **2017**, *121* (5), 2968–2986.
- (18) Faleiro, J. H.; Dantas, N. O.; Silva, A. C. A.; Barbosa, H. P.; da Silva, B. H. S. T.; Lima, K. de O.; Gonçalves, R. R.; Ferrari, J. L. Niobium Oxide Influence in the Phosphate Glasses Triply Doped with Er³⁺/Yb³⁺/Eu³⁺ Prepared by the Melting Process. *J. Non Cryst. Solids* **2021**, *571*, No. 121051.
- (19) Kamalaker, V.; Chanakya, N.; Madhuri, J. H.; Jahangeer, N.; Reddy, M. M.; Ramesh, C.; Muralikrishna, P.; Upender, G. Influence of Nb⁵⁺ and La³⁺ Ions on Physical Properties of the Quaternary TeO₂-ZnO-Nb₂O₅-La₂O₃ Glass System. *Ceram. Int.* **2024**, *50* (21), 41472–41482.
- (20) Komatsu, T.; Honma, T.; Tasheva, T.; Dimitrov, V. Structural Role of Nb₂O₅ in Glass-Forming Ability, Electronic Polarizability and Nanocrystallization in Glasses: A Review. *J. Non Cryst. Solids* **2022**, *581*, No. 121414.
- (21) Makuła, P.; Pacia, M.; Macyk, W. How To Correctly Determine the Band Gap Energy of Modified Semiconductor Photocatalysts Based on UV–Vis Spectra. *J. Phys. Chem. Lett.* **2018**, 9 (23), 6814–6817.
- (22) Miguez, M. L.; Barbano, E. C.; Coura, J. A.; Zílio, S. C.; Misoguti, L. Nonlinear Ellipse Rotation Measurements in Optical Thick Samples. *Appl. Phys. B* **2015**, *120* (4), 653–658.
- (23) Milam, D. Review and Assessment of Measured Values of the Nonlinear Refractive-Index Coefficient of Fused Silica. *Appl. Opt.* **1998**, 37 (3), 546–550.
- (24) Miguez, M. L.; Barbano, E. C.; Zilio, S. C.; Misoguti, L. Accurate Measurement of Nonlinear Ellipse Rotation Using a Phase-Sensitive Method. *Opt. Express* **2014**, 22 (21), 25530–25538.
- (25) da Silva, L. O. E.; Silva, L. D.; Zanotto, E. D.; de Oliveira Junior, M.; Manzani, D. Alkaline Earth Metal Fluorides (MgF₂, CaF₂,

- SrF₂, BaF₂) and Nb₂O₅ Effect on the Structural and Optical Properties of New Fluorophosphoniobate Glasses. ACS Omega 2025.
- (26) Clabel H, J. L.; Lozano C, G.; Chacaliaza-Ricaldi, J.; Mastelaro, V. R.; Mendonça, C. R.; Messaddeq, Y.; Marega, E.; Rivera, V. A. G. Nonlinear Optical Properties in Pr³⁺-Er³⁺-Codoped Tellurite Glasses. *Mater. Res. Bull.* **2024**, *177*, No. 112832.
- (27) Eevon, C.; Halimah, M. K.; Zakaria, A.; Azurahanim, C. A. C.; Azlan, M. N.; Faznny, M. F. Linear and Nonlinear Optical Properties of Gd³⁺ Doped Zinc Borotellurite Glasses for All-Optical Switching Applications. *Results Phys.* **2016**, *6*, 761–766.
- (28) Chandrashekaraiah, G.; Reddy, N. S.; Sujatha, B.; Viswanatha, R.; Reddy, C. N. Role of Er³⁺ and Bi³⁺ Ions on Thermal and Optical Properties of Li₂B₄O₇ Glasses: Structural Correlation. *J. Non Cryst. Solids* **2018**, 498, 252–261.
- (29) Chu, C. M.; Wu, J. J.; Yung, S. W.; Chin, T. S.; Zhang, T.; Wu, F. B. Optical and Structural Properties of Sr–Nb–Phosphate Glasses. *J. Non Cryst. Solids* **2011**, 357 (3), 939–945.
- (30) Marcondes, L. M.; Maestri, S.; Sousa, B.; Gonçalves, R. R.; Cassanjes, F. C.; Poirier, G. Y. High Niobium Oxide Content in Germanate Glasses: Thermal, Structural, and Optical Properties. *J. Am. Ceram. Soc.* **2018**, *101* (1), 220–230.
- (31) Pelosi, A. G.; Santos, S. N. C.; Dipold, J.; Andrade, M. B.; Hernandes, A. C.; Almeida, J. M. P.; Mendonça, C. R. Effects of Modifier Oxides in the Nonlinear Refractive Index of Niobium-Borotellurite Glasses. *J. Alloys Compd.* **2021**, 878, No. 160382.
- (32) Cao, X.; Wan, R.; Li, X.; Guo, C.; Tian, S.; Wang, P. Modulating the Nonlinear Refractive Index through F/O Ratio to Reduce the Self-Focusing Effect of Fluorophosphate Glasses. *Opt. Express* **2025**, 33 (3), 6254–6267.
- (33) Mošner, P.; Hostinský, T.; Koudelka, L. Thermal, Structural and Crystallization Study of Na₂O-P₂O₅-Nb₂O₅ Glasses. *J. Solid State Chem.* **2022**, *316*, No. 123545.
- (34) Sene, F. F.; Martinelli, J. R.; Gomes, L. Optical and Structural Characterization of Rare Earth Doped Niobium Phosphate Glasses. *J. Non Cryst. Solids* **2004**, *348*, 63–71.
- (35) Santos, S. N. C.; Paula, K. T.; Almeida, J. M. P.; Hernandes, A. C.; Mendonça, C. R. Effect of Tb³⁺/Yb³⁺ in the Nonlinear Refractive Spectrum of CaLiBO Glasses. *J. Non Cryst. Solids* **2019**, 524, No. 119637.
- (36) Misoguti, L.; Kassab, L. R. P.; Bordon, C. D. S.; Rodrigues, J. J.; Alencar, M. A. R. C. Nonlinear Refraction and Absorption Spectroscopy of Tellurite Glasses within Telecom Bands. *J. Alloys Compd.* **2021**, 872, No. 159738.
- (37) Jagannath, G.; Eraiah, B.; Gaddam, A.; Fernandes, H.; Brazete, D.; Jayanthi, K.; Krishnakanth, K. N.; Rao, S. V.; Ferreira, J. M. F.; Annapurna, K.; Allu, A. R. Structural and Femtosecond Third-Order Nonlinear Optical Properties of Sodium Borate Oxide Glasses: Effect of Antimony. *J. Phys. Chem. C* **2019**, *123* (9), 5591–5602.
- (38) Keshavamurthy, K.; Swetha, B. N.; Al-Harbi, F. F.; G, J.; Almuqrin, A. H.; Sayyed, M. I.; Ahmed, S. Ben.; Pramod, A. G.; Itigi, S.; P, R.; Patwari, D. R.; Murthy, N. L.; Sathish, K. N.; Rao, S. V. Improved Near-infrared Nonlinear Optical Properties of Sm³⁺ Containing Borate Glasses: Effect of Silver Nanoparticles Concentration. *Opt Mater.* **2021**, *122*, No. 111804.
- (39) Li, Q.; Yuan, X.; Jiang, X.; Wang, J.; Liu, Y.; Zhang, L. Femtosecond-Scale All-Optical Switching in Oxyfluorogallate Glass Induced by Nonlinear Multiphoton Absorption. *RSC Adv.* **2021**, *11* (51), 32446–32453.
- (40) Clabel H, J. L.; Valverde, J. V. P.; Lozano C, G.; Marega, E.; Mastelaro, V. R.; Mendonça, C. R. Nonlinear Optical Properties of La³⁺-Doped Tellurite-Zinc Glasses: Impact of Chemical Bonding and Physical Properties via Raman and XPS. *Ceram. Int.* **2025**, *51* (1), 844–855.
- (41) Azlan, M. N.; Halimah, M. K.; Suriani, A. B.; Azlina, Y.; El-Mallawany, R. Electronic Polarizability and Third-Order Nonlinearity of Nd³⁺ Doped Borotellurite Glass for Potential Optical Fiber. *Mater. Chem. Phys.* **2019**, 236, No. 121812.

- (42) Pintori, G.; Cattaruzza, E. XPS/ESCA on Glass Surfaces: A Useful Tool for Ancient and Modern Materials. *Opt Mater: X* **2022**, 13, No. 100108.
- (43) York-Winegar, J.; Harper, T.; Brennan, C.; Oelgoetz, J.; Kovalskiy, A. Structure of SnF₂-SnO-P₂O₅ Glasses. *Phys. Procedia* **2013**, *44*, 159–165.
- (44) Teterin, Yu. A.; Nefedov, V. I.; Churbanov, M. F.; Teterin, A. Yu.; Maslakov, K. I.; Zorin, E. V. X-Ray Photoelectron Study of Te-W-O and Te-W-La-O Glasses. *Inorg. Mater.* **2007**, 43 (8), 888–896.
- (45) Chowdari, B. V. R.; Tan, K. L.; Chia, W. T.; Gopalakrishnan, R. X-Ray Photoelectron Spectroscopic Studies of Molybdenum Phosphate Glassy System. J. Non Cryst. Solids 1990, 119 (1), 95–102.
- (46) Chen, C.; Jiang, Y.; Zhang, L.; Guan, F.; Wang, Z.; Huang, X.; Zeng, H.; Yuan, X.; Zhang, L.; He, J. Luminescence and Structural Evolution in Ultra-low Melting Quaternary Tin Fluorophosphate Glasses (NaF-SnF₂ -SnO-P₂O₅). *J. Am. Ceram. Soc.* **2022**, *105* (4), 2595–2604.
- (47) Huang, T.; Hao, Z.; Gong, H.; Liu, Z.; Xiao, S.; Li, S.; Zhai, Y.; You, S.; Wang, Q.; Qin, J. Third-Order Nonlinear Optical Properties of a New Copper Coordination Compound: A Promising Candidate for All-Optical Switching. *Chem. Phys. Lett.* **2008**, 451 (4–6), 213–217.



CAS BIOFINDER DISCOVERY PLATFORM™

STOP DIGGING THROUGH DATA —START MAKING DISCOVERIES

CAS BioFinder helps you find the right biological insights in seconds

Start your search

